



HAL
open science

Neovascularization Detection in Diabetic Retinopathy from Fluorescein Angiograms

Benjamin Béouche-Hélias, David Helbert, Cynthia de Malézieu, Nicolas
Leveziel, Christine Fernandez-Maloigne

► **To cite this version:**

Benjamin Béouche-Hélias, David Helbert, Cynthia de Malézieu, Nicolas Leveziel, Christine Fernandez-Maloigne. Neovascularization Detection in Diabetic Retinopathy from Fluorescein Angiograms. *Journal of Medical Imaging*, 2017, 4 (4), pp.044503. 10.1117/1.JMI.4.4.044503 . hal-01625993

HAL Id: hal-01625993

<https://hal.science/hal-01625993>

Submitted on 3 Apr 2018

HAL is a multi-disciplinary open access archive for the deposit and dissemination of scientific research documents, whether they are published or not. The documents may come from teaching and research institutions in France or abroad, or from public or private research centers.

L'archive ouverte pluridisciplinaire **HAL**, est destinée au dépôt et à la diffusion de documents scientifiques de niveau recherche, publiés ou non, émanant des établissements d'enseignement et de recherche français ou étrangers, des laboratoires publics ou privés.

Neovascularization Detection in Diabetic Retinopathy from Fluorescein Angiograms

Benjamin Béouche-Hélias^a, David Helbert^{b,*}, Cynthia de Malézieu^a, Nicolas Leveziel^a, Christine Fernandez-Maloigne^b

^aDepartment of Ophthalmology, CHU Poitiers, 2 rue de la Milétrie, BP 577,86021 Poitiers cedex, France

^bXLIM, CNRS U-7252, University of Poitiers, 11 Bd Marie et Pierre Curie, BP 30179 86962 Futuroscope Chasseneuil Cedex, France

Abstract. Even if a lot of work has been done on Optical Coherence Tomography (OCT) and color images in order to detect and quantify diseases such as diabetic retinopathy, exudates or neovascularizations, none of them is able to evaluate the diffusion of the neovascularizations in retinas. Our work has been to develop a tool able to quantify a neovascularization and the fluorescein leakage during an angiography. The proposed method has been developed following a clinical trial protocol, images are taken by a Spectralis (Heidelberg Engineering). Detections are done using a supervised classification using specific features. Images and their detected neovascularizations are then spatially matched by an image registration. We compute the expansion speed of the liquid that we call *diffusion index*. This last one specifies the state of the disease and permits to indicate the activity of neovascularizations and allows a follow-up of patients. The method proposed in this paper has been built to be robust, even with laser impacts, to compute a diffusion index.

Keywords: Diabetic retinopathy, neovascularization, classification, anti-VEGF, diabetes.

*David Helbert, david.helbert@univ-poitiers.fr

1 Introduction

The detection and follow-up of diabetic retinopathy, an increasingly important cause of blindness, is a public health issue. Indeed, loss of vision can be prevented by early detection of diabetic retinopathy and increased monitoring by regular examination. There are now many algorithms for the automatic detection of common anomalies of the retina (microaneurysms, haemorrhages, exudates, tasks, ...). However, very few researches have been done on the detection of a major pathology, which is neovascularization, corresponding to the growth of new blood vessels due to a large lack of oxygen in the retinal capillaries.

Our work has not been to substitute manual detections of experts but to help them doing it by suggesting what areas of the retina could or not be considered as having neovascularizations (NVs) and by providing quantitative and qualitative proliferative diabetic retinopathy such as the area of NV, the location to the optical nerve, the activity of NV (diffusion index). The main goal has been to provide a diffusion index of the injected fluorescent liquid, which indicates the severity of the pathology, to follow the patient over the years.

Diabetic retinopathies is one of the first cause of visual impairment worldwide, due to the increasing incidence of diabetes. Proliferative diabetic retinopathy (PDR) is defined by the outgrowth of preretinal vessels leading to retinal complication *i.e.* intravitreal hemorrhages and retinal detachments. Today the laser photocoagulation is the standard of care treatment of proliferative diabetic retinopathy, leading to a decrease of growth factors secretion in photoagulated areas of the retina.

Vascular endothelial growth factor (VEGF) is responsible of the growth of healthy vessels, but also of the NVs due to diabetes. Research is active on finding a specific type of anti-VEGF that could stop the growth of the NVs specifically. A clinical trial (ClinicalTrials.gov Identifier: NCT02151695), called "Safety and Efficacy of Aflibercept in Proliferative Diabetic Retinopathy" is in progress at the CHU of Poitiers, testing the effects of a specific anti-VEGF : Aflibercept. This drug has been approved by the European Medicines Agency (EMA) and the United States Food and Drug Administration (FDA) for treatment of exudative age-related macular degeneration, another retinal disease characterized by choroidal new vessels. The aim of this pilot study is to evaluate the efficacy and the safety of Aflibercept intravitreal injections compared to panretinal photocoagulation for proliferative diabetic retinopathy.

In ophthalmology, the majority of the works on the retinal diseases is about the detection of the exudates,³⁻⁷ the healthy vessels segmentation,⁸⁻¹⁰ the detection of the neural disk^{11,12} but none of them is about the detection of the proliferative diabetic retinopathy within angiograms.

Some works have also been done on the image registration for retinal images. Can¹³ *et al* have proposed the registration of a pair of retinal images by using branching points and cross-over points in the vasculature. Zheng *et al* have developed in¹⁴ a registration algorithm by using salient feature region description. Legg *et al* have illustrated in¹⁵ the efficiency of mutual information for registration of fundus colour photographs and colour scanning laser ophthalmoscope images.

Few steps are needed to compute that diffusion index. It is a growth in time which means that we have to detect and quantify the pathology on both injection times and compare their area. As it is nearly impossible to have exactly the same conditions during the acquisition (eye movements, focus of the camera, angle), we need an image registration to have an estimation of deformations and to correctly spatially correlate NVs. For the segmentation, we used a supervised classification by Random Forests¹⁶ using intensity, textural and contextual features, and a database of trained images from the clinical trials. These steps are shown in Fig. 1.

The paper is organized as follows. In section 2 we present the microscope and the acquisition protocol. The

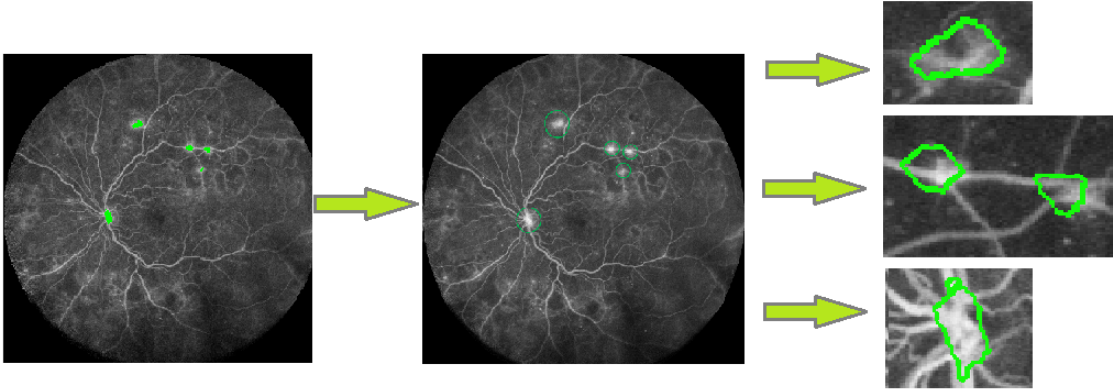


Fig 1: Example of a full detection by our method.

image registration on both injection times is proposed in section 3. We then propose a novel neovascularization detection method in section 4 and an automatic diffusion index computation in section 5.

2 Materials

Our database is made of images taken by the ©Spectralis Heidelberg Engineering microscope with an ultra-widefield lens covering a 102° field of view. It delivers undistorted images of a great part of the retina, making the detection easier and monitor abnormal peripheral changes.

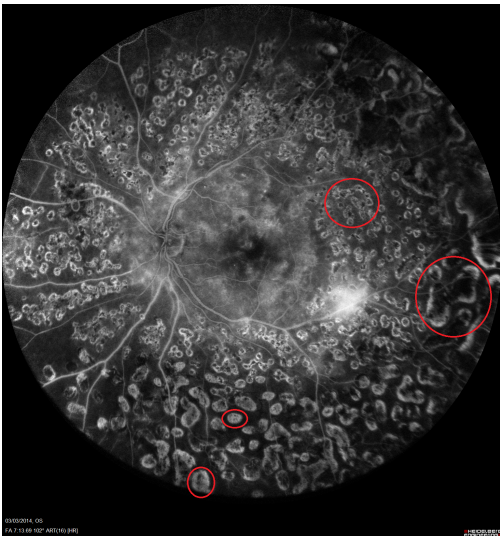


Fig 2: Image of an angiogram taken with the Heidelberg Spectralis. Laser impacts are present all over the image, some examples are highlighted in red.

Images are in gray levels, the areas that are bright are mainly 1/ those leaking during fluorescein angiography due to NV, 2/ normal retinal vessels or 3/ laser impacts. Some images we have taken from patients who have been treated by laser photocoagulation, visible on Fig. 2. These

impacts are annoying because they are also very bright for some parts. The blood still spread through some impacts, and can be big enough to be wrongly assimilated to a NV.

To qualify the PDR by the index leakage, different times of acquisition during fluorescein angiography were used. The protocol presented below is the clinical trial's protocol which is composed of two image acquisitions:

1. fluorescein injection into the patient's arm;
2. acquisition of the early time injection (t_0);
3. acquisition of the late time injection (t_f).

The few minutes left between different acquisitions times allow visualization of the fluorescein leakage defined as a progressive increase of the NV area with blurring edges of the NV. No leakage is observed on normal retinal vessels. On Fig. 3 we can see pictures of the same eye with acquisitions at t_0 and t_f , where we can see the fluorescein spreading first into arteries and then bleeds in neovascularizations.

As images are taken by three minutes, some spatial differences occur and we need to spatially correlate both images with an image registration which is presented in the next part.

15 diabetic patients were included in the analysis and ophthalmologists have identified 60 different NV from fluorescein angiographies on wide field imaging.

3 Image registration

The image registration does not aim to be perfect but to allow spatial comparison between NV taken in both images to compute quantitative data. The best registration model should be a local method, but for that reason just explained, a global method is widely enough for the comparison. Some of them are very popular and have been tested by many experts like Scale Invariant Feature Transform (SIFT),¹⁷ Maximally Stable Extremal Regions (MSER)¹⁸ or Speeded Up Robust Features (SURF).¹⁹ We found that

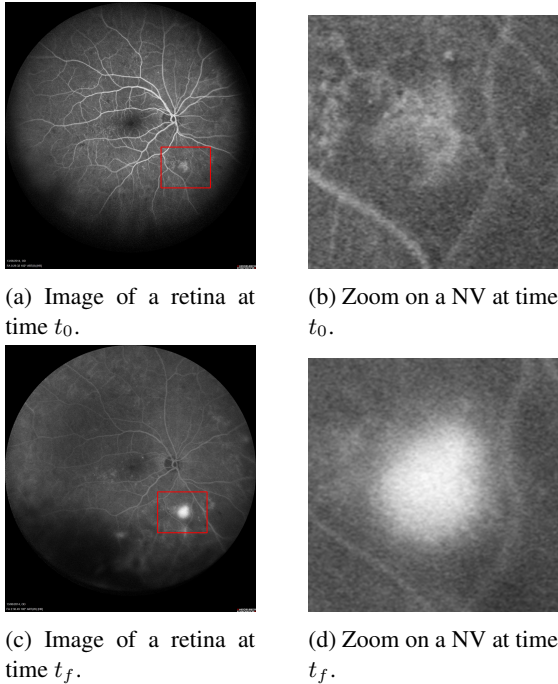


Fig 3: Retina acquired at initial time t_0 and final time t_f .

SIFT was robust and fast enough for the deformations we have on images.

3.1 Constraints

Images are taken with a manually movable camera with no spacial landmarks to help. Moreover the eye of the patient slightly moves between each capture, even when focusing a specific direction, which means that the images for the two injection times can be geometrically different, with translations (x and y), scaling (z) and some small rotations (θ).

Futhermore, tissues on the retina can slightly be different over the time, depending on several biological factors, like the heat, the light or the blood flood. We then have global and local geometrical deformations. The brightness of the images mainly depends on the diffusion of the fluorescent liquid injected in the patient. Some tissues will appear more or less bright between both images and sometimes will simply be or not present onto them. For example, healthy arteries will appear darker on the late time injection because the liquid first flood into them (t_0) and then spread into different tissues like neovessels (t_f). That is why NVs appear brighter and are easier to detect on t_f . We finally have global colorimetry changes, which impact on the general contrast of the image, and very local changes.

3.2 Deformation computation

First steps are the extraction and the description of keypoints on the image. These keypoints need to be invari-

ant to image scaling and rotation, and mostly invariant to change in illumination, they also need to be highly distinctive by their description to be matched further.

To match the extracted keypoints, we use the brute force method. For each keypoint we take the two nearest points in terms of Euclidean distance and we only keep those who the first nearest point is inferior to 0.8 times the second nearest neighbor (as proposed in¹⁷).

The deformation matrix is finally computed by the RANSAC algorithm (Random Sample Consensus).²⁰

3.3 Results and discussion

We know that deformations we have between both images are relatively small. Even with small movements from the eye or the camera, the lens used takes wide images enough to avoid big deformations because it makes the margin of movement very small, so we removed matching points that obviously are too far from each other. Within the accordance of the experts and the visualization of the different images, we set the distance threshold to a ratio (r) of the diagonal of the image, where r is the constant set which can be adjusted depending on the strength of the deformations. For example, you can set r to 0.5 if you want to set the threshold at half the length of the diagonal. We can see on Fig. 4 that the registration process works well. It is still a global image registration that could be more precise with a specific local non rigid algorithm, but the aim is to pair NVs and be spatially correct when comparing the leakage areas, so we do not need to have a perfect registration.

Once the image registration is done, we can process both images. The segmentation method we used is explained in the next part.

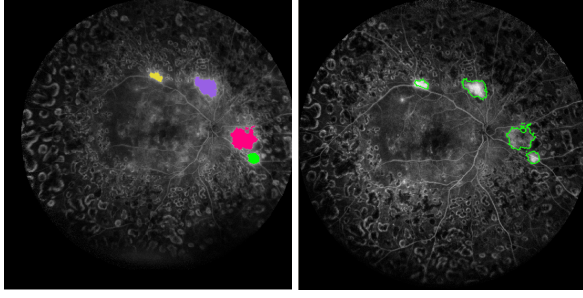
4 Neovascularizations detection

4.1 Principle

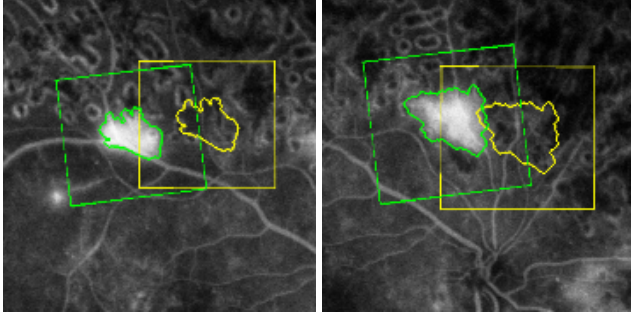
The aim of a supervised classification is to set the rules that will let the algorithm classify objects into classes from features describing these objects. The algorithm is first trained with a portion of the available data to learn the classification rules (see Fig. 5).

As supervised classification tends to give better results when it is possible to have a good trained database we choose to use the Random Forests of decision trees¹⁶ (RF), which is a supervised classification algorithm that gives good results even with a small database.

The noise is very high in most images, notably the laser impacts that some patients can have (see Fig. 2). They have some close properties like the brightness that is very high and sometimes have the same shape and size. Some noise is also due to the acquisition itself : eyelashes can blur a part of the images and the automated settings of the camera can lead to more or less blur just as examples.



(a) Detected NVs on t_f . (b) NVs from t_f after image registration on t_0 .



(c) Example of NVs with their bounding boxes. Yellow box is the original box, the green box is the deformed box.

Fig 4: Registration of the NVs from a t_f image to a t_0 image.

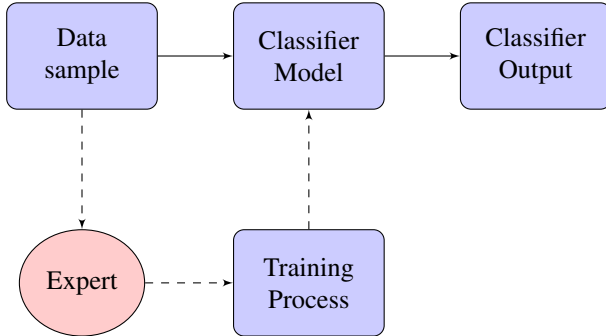


Fig 5: Supervised classification process.

4.2 Classification Algorithm

4.2.1 Features

Supervised classification can be used with as many features as we want but can be poor if too many bad features are used. To prune the features, it is possible to use multiple features and try to see which are the best by some tests. Once you have found the most important features, you can decide if you want to get rid of the other features or not, depending of your needs in terms of accuracy and time computation. Note that images being only in gray level.

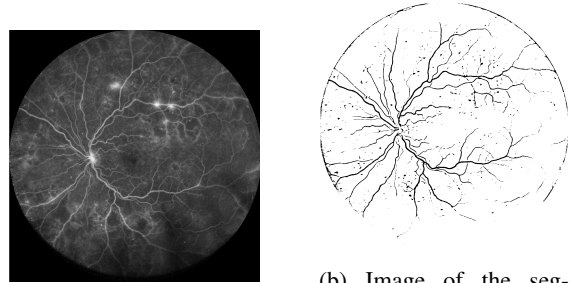
We choose to take enough features to prune our selection because our database is not big enough to take on many features and still be a good predicate. NVs being

very bright, we choose to have several features based on the intensity, we also add textural and one contextual features as listed below.

Intensity Because leakages are bright, we put a lot of weight onto the features based on the intensity : mean, maximum and minimum intensity in the neighborhood. We also take in account the single value of the classified pixel. The values are normalized. Mean, maximum and minimum values are computed in a 5×5 and a 9×9 neighborhood, which leads to six features.

Texture Texture can be a discriminator between laser impacts and NVs because laser impacts are more likely heterogeneous than the second one. For that, we calculate the variance on a 5×5 and a 9×9 neighborhood. We compute an isotropic gradient with a 3×3 and 5×5 Sobel operator. We add some Haralick's texture features: angular second moment, contrast and correlation.²¹

Contextual Contextual features are very important because the intensity is often not enough and is very sensitive to the noise. We add a vessel segmentation in our process, which we translate into a feature. Healthy vessels could sometimes be classified as NVs if we only take into account the intensity features because they are very similar. We base our method on the method proposed in.¹⁰ It is a morphological segmentation based on the width and the homogeneity of the vessels and weighted by the luminance. See figure 6.



(a) Non computed image (b) Image of the segmented vessels

Fig 6: Detection of the healthy vessels.

With our dataset, the importance of the proposed features are listed on Fig. 7 (values have been rounded for visibility). The most important features are the minimum intensity and the mean intensity in the 9×9 neighborhood. As expected the intensity of the classified pixel is poor because several noise is also bright (e.g laser impacts and healthy vessels).

Fig. 8 is an example of a classification with the Random Forests algorithm. Compared to the ground truth, the true positives are in green, false positives in red, false negatives in blue and true negatives in white.

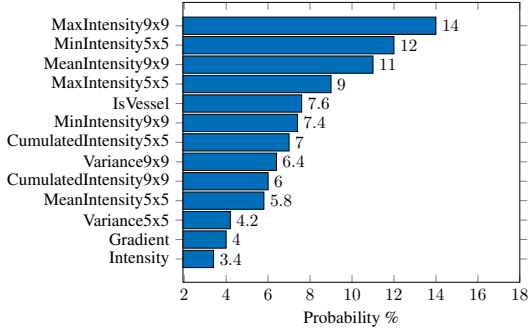
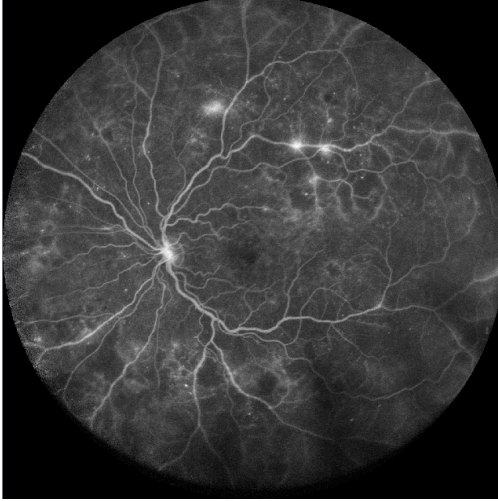
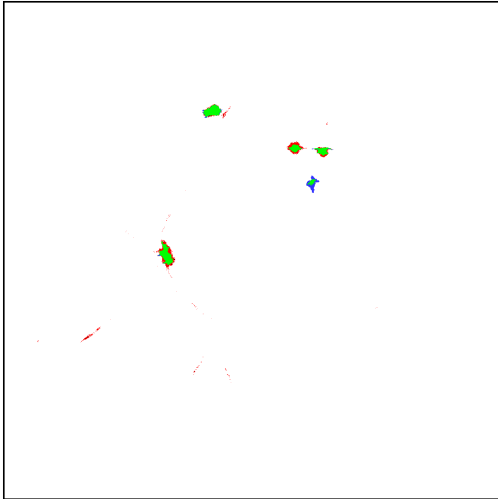


Fig 7: List of the feature importance.



(a) Original image



(b) Result of the supervised classification

Fig 8: Result of the RF classification on an image. Green regions represent the true positives, red regions the false positives and blue the false negatives.

4.3 Post processing

Because it is a pixel-wise classification, it is not sufficient enough by itself to have compact and fulfilled regions, so

we added few post-treatments.

As the leakage is almost isotropic in the vitreous, it is correct to compare the leakage with a cloud that is more or less dense but mostly filled (i.e without holes). Classification sometimes gives regions with little holes that can easily be filled with a closing operation by mathematical morphology. Moreover some thin line detections can happen onto laser impacts edges or healthy vessels for example, we can remove them with an opening operation.

Thus, after the classification, a morphological closing and a morphological opening are directly applied to remove thin false detections and they fill the holes of the detected NVs.

4.4 Results and discussion

Random forests algorithm gives a probability for each pixel to belong to the class "NV" or to the class "other". Because the results may vary due to the probabilities, we tried the algorithm with different thresholds (λ) of probability. Results are obtained using a cross validation process on our database. For each image, the training set is composed of all the data except those extracted from the current image. In this way the data of the image are not taken into account for the training and the statistical model is not wrongly influenced.

As results, we compare expert manual and automated segmentation to classify the resulting pixels into four classes : true positive (TP), false positive (FP), true negative (TN) and false negative (FN).

Given these classes, we can calculate the sensibility (S), the specificity (Sp) and the pixel prediction value (PPV) as following:

$$S = \frac{TP}{TP + FN} \quad (1)$$

$$Sp = \frac{TN}{FP + TN} \quad (2)$$

$$PPV = \frac{TP}{TP + FP} \quad (3)$$

However, NVs are mainly small compared to the size of the image and results in a big disparity between the number of positive and negative pixels. The specificity is then always very close to 1 because the pixel number belonging to the background is too much compared to the positives, so we neglecte this feature from our results.

4.4.1 Detection at t_f

Results of the detection for the t_f images are given in the figure 9. We can see that the pixel prediction value is very influenced by probability threshold λ compared to the sensibility which is less influenced. A λ under 0.8 gives a good detection of the NVs (high S , but very poor PPV). When the λ is above 0.8, the S decreases a bit but

stays very high, whereas the *PPV* becomes more reliable around a λ of 0.8 and becomes $> 90\%$ for a λ superior to 0.9.

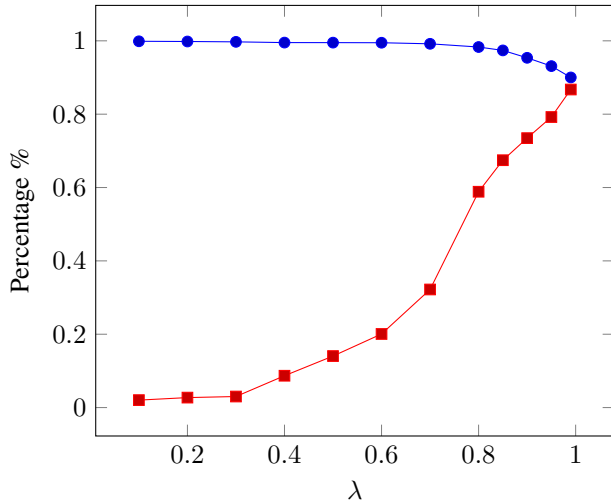


Fig 9: Sensibility (blue dots) and Pixel Prediction Value (red squares) results for the classification on t_f depending on λ used for the probabilities.

4.4.2 Detection at t_0

Results of the detection for the t_0 images are given in the figure 10. They are not as high as for the T_F images, as expected, because it is not easy to distinguish them from healthy vessels before the big part of the spread. As for the t_f images, *PPV* is very poor below a λ of 0.8 and becomes very high above. The problem is that above this threshold, the *S* decreases more than expected, until 60% for a 0.99 λ .

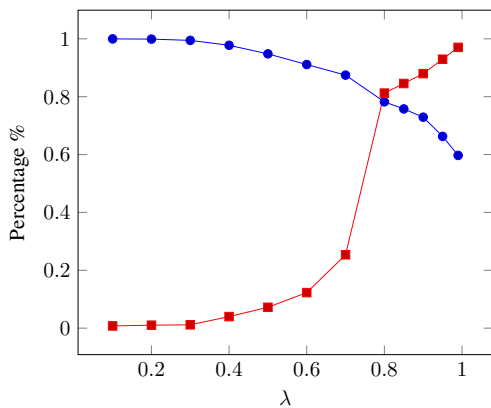


Fig 10: Sensibility (blue dots) and Pixel Prediction Value (red squares) results for the classification on t_0 depending on λ used for the probabilities.

5 Diffusion index

5.1 Methodology and Results

The diffusion index has to give an indication about the severity of the diabetic retinopathy, which means that it has to compare two liquid spread volumes. As we only work with two dimension images, we can only guess that the spreading is isotropic and that an index computed only with the surface is enough to tell the strength of the leakage.

Figure 11 recalls the processing: we detect the NV surfaces at time t_f and inside these surfaces, we detect NV surfaces at time t_0 . The diffusion index is then computed by the differentiation of NV areas at t_0 and at t_f .

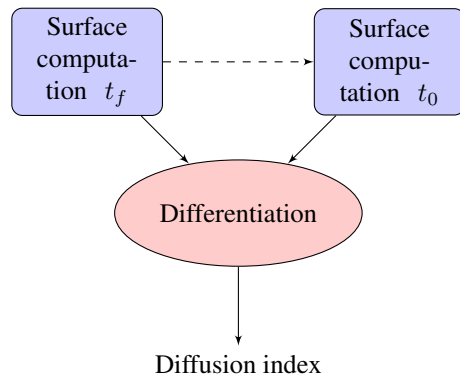


Fig 11: Methodology of diffusion index computation.

5.2 Results ans discussion

The detection of NVs into the t_0 and t_f images is quite complex and really depends on many parameters. The parameters are linked to the fact that the eyes of the patient moves between each capture and the images between two injections can be geometrically different.

Computed diffusion indices are close to the ground truth (cf Tab. 1), indeed the error is only 0.1 or 0.5%.

| | Ground Truth | Automated | Difference |
|----------|--------------|-----------|------------|
| Mean | 2.09 | 2.10 | 0.01 |
| σ | 0.33 | 0.54 | 0.52 |

Table 1: Diffusion index results.

Moreover the retina can slightly be different the time, depending biological factors, and the healthy arteries appear darker according the time of the capture.

In our experience, for neovascularization of diabetic retinopathy, the algorithm shows a sensibility and pixel predictive values are effective to describe lesions.

The detection of NVs onto the t_0 images is quite complex and really depends on many parameters. We obtain a low Mean Square Error for probability λ equal to 0.8.

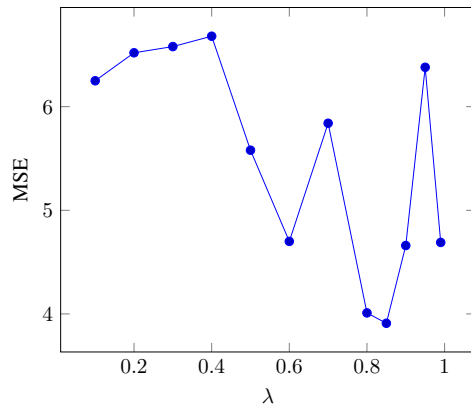


Fig 12: Mean Square Errors for each computed diffusion index according to probability threshold λ used for the classification.

6 Conclusion

We propose to compute diffusion indices after detecting neovascularizations in noisy angiogram images at initial time t_0 and at final time t_f . First we extract the NV areas at time t_f and we use the area to detect the NV areas at time t_f . We also need to register images between the two acquisitions and we choose to detect interest points using SIFT and we estimate the geometrical transformation for each neovascularization.

To detect neovascularizations, we learn features which characterize the NV. We so choose a random tree forest and this approach gives good detection results and the computed diffusion index is close to the ground truth.

A clinical study about this algorithm and manual method is now necessary to compare them, to permit the evaluation of clinical effectiveness and to propose a software solution for the ophthalmologists.

Acknowledgments

This research is financially supported by the clinical trial (ClinicalTrials.gov Identifier: NCT02151695) called "Safety and Efficacy of Aflibercept in Proliferative Diabetic Retinopathy" in progress at the CHU of Poitiers, France. The authors state no conflict of interest and have nothing to disclose.

References

- 1 F. Dong and J. Peng, "Brain mr image segmentation based on local gaussian mixture model and nonlocal spatial regularization," *Journal of Visual Communication and Image* (2014).
- 2 J. Zhang, K. Ma, and M. H. Er, "Tumor segmentation from magnetic resonance imaging by learning via one-class support vector machine," *International Workshop on Advanced Image Technology* (2004).
- 3 X.Zhang, G. Thibault, E. Decencire, *et al.*, "Exudate detection in color retinal images for mass screening of diabetic retinopathy," *Medical Image Analysis* (2014).
- 4 M. Niemeijer, B. Ginneken, S. Russel, *et al.*, "Automated detection and differentiation of drusen, exudates, and cotton-wool spots in digital color fundus photographs for early diagnosis of diabetic retinopathy," *Invest Ophthalmol Vis Sci.* (2009).
- 5 M. Abramoff, M. Niemeijer, and S. Russel, "Automated detection of diabetic retinopathy: barriers to translation into clinical practice," *Investigative Ophthalmology and Visual Science* (2011).
- 6 A. Osareh, M. Mirmehdi, B. Thomas, *et al.*, "Automated identification of diabetic retinal exudates in digital colour images," *British Journal of Ophthalmology* (2003).
- 7 E. Imani, H.-R. Pourreza, and T. Banaee, "Fully automated diabetic retinopathy screening using morphological component analysis," *Computerized Medical Imaging and Graphics* (2015).
- 8 J. Staal, M. Abramoff, M. Niemeijer, *et al.*, "Ridge-based vessel segmentation in color images of the retina," *IEEE Transactions on Medical Imaging* (2004).
- 9 A. Mendona and A. Campilho, "Segmentation of retinal blood vessels by combining the detection of centerlines and morphological reconstruction," *IEEE Transactions on Medical Imaging* (2006).
- 10 U. Nguyen, A. Bhuiyan, L. Park, *et al.*, "An effective retinal blood vessel segmentation method using multi-scale line detection," *Pattern Recognition* (2013).
- 11 C. Sinthanayothin, J. Boyce, H. Cook, *et al.*, "Automated localisation of the optic disc, fovea, and retinal blood vessels from digital colour fundus images," *British Journal of Ophthalmology* (1999).
- 12 C. Duangate, B. Uyyanonvara, S. Makhanov, *et al.*, "Parameter-free optic disc detection," *Computerized Medical Imaging and Graphics* (2011).
- 13 A. Can, C. V. Stewart, B. Roysam, *et al.*, "A feature-based, robust, hierarchical algorithm for registering pairs of images of the curved human retina," *Transactions on Pattern Analysis and Machine Intelligence* (2002).
- 14 J. Zheng, J. Tian, K. Deng, *et al.*, "Salient feature region: a new method for retinal image registration," *Information Technology in Biomedicine, IEEE Transactions on* **15**(2), 221–232 (2011).
- 15 P. A. Legg, P. L. Rosin, D. Marshall, *et al.*, "Improving accuracy and efficiency of mutual information for multi-modal retinal image registration using

- adaptive probability density estimation,” *Computerized Medical Imaging and Graphics* **37**(7), 597–606 (2013).
- 16 L. Breiman, “Random forests,” *Machine Learning* (2001).
 - 17 D. G. Lowe, “Distinctive image features from scale-invariant keypoints,” *International Journal of Computer Vision* (2004).
 - 18 P. Forssen and D. Lowe, “Shape descriptors for maximally stable extremal regions,” *Computer Vision, 2007. ICCV 2007. IEEE 11th International Conference* (2007).
 - 19 H. Bay, T. Tuytelaars, and L. V. Gool, “Surf : speeded up robust features,” *Computer Vision and Image Understanding* (2008).
 - 20 M. A. Fischler and R. C. Bolles, “Random sample consensus : A paradigm model fitting with applications to image analysis and automated cartography,” *Communications of the ACM* (1981).
 - 21 K. S. Robert M. Haralick, “Textural features for image classification,” *IEEE Transactions on systems, man, and cybernetics* (1973).